Inorganic Chemistry

Article

pubs.acs.org/IC

Self-Assembled Tetra- and Pentanuclear Nickel(II) Aggregates From Phenoxido-Based Ligand -Bound {Ni_2} Fragments: Carboxylate Bridge Controlled Structures

Aloke Kumar Ghosh,[†] Michael Shatruk,[‡] Valerio Bertolasi,[§] Kausikisankar Pramanik,[∥] and Debashis Ray*[,†]

[†]Department of Chemistry, Indian Institute of Technology, Kharagpur 721 302, India

[‡]Department of Chemistry & Biochemistry, Florida State University, Tallahassee, Florida 32306, United States

[§]Dipartimento di Scienze Chimiche e Farmaceutiche, Centro di Strutturistica Diffrattometrica, Università di Ferrara, via L. Borsari 46, 44100 Ferrara, Italy

[∥]Inorganic Chemistry Section, Department of Chemistry, Jadavpur University, Kolkata-70032, India

Supporting Information

ABSTRACT: Three different carboxylato bridges (R = C_2H_5, CF_3, and $PhCH_2$ in RCO_2^-) have been used to obtain the supramolecular aggregates $[Ni_5(\mu\text{-}H_2bpmp)_2(\mu_3\text{-}OH)_2(\mu_{1,3}\text{-}O_2CC_2H_5)_6]\cdot 2H_2O\cdot 4DMF$ (**1**·$2H_2O$·4DMF), $[Ni_4(\mu_3\text{-}H_2bpmp)_2(\mu_3\text{-}OH)_2(\mu_{1,3}\text{-}O_2CCF_3)_2](CF_3CO_2)_2\cdot H_2O$ (**2**·H_2O), and $[Ni_4(\mu_3\text{-}H_2bpmp)_2(\mu_3\text{-}OH)_2(\mu_{1,3}\text{-}O_2CCH_2Ph)_2]\text{-}(PhCH_2CO_2)_2\cdot 4H_2O$ (**3**·$4H_2O$) (H_3bpmp =2,6-bis-[(3-hydroxy-propylimino)-methyl]-4-methyl-phenol) from the hydroxido-bridged dinuclear motif $[Ni_2(\mu\text{-}H_2bpmp)(OH)]^{2+}$. These complexes have been characterized by X-ray crystallography and magnetic measurements. A change from propanoate group to trifluoroacetate and phenylaceate groups provided different course of cluster assembly based on $Ni_2(\mu\text{-}H_2bpmp)_2$ fragments. The $\{Ni_5(\mu_3\text{-}OH)_2(\mu_{1,3}\text{-}O_2CC_2H_5)_6\}^{2+}$ core in **1** contains five Ni^{II} ions in an hourglass (pentanuclear vertex-shared double cubane) arrangement. These compounds are new examples of $[Ni_5]$ and $[Ni_4]$ complexes where aggregation of the building motifs are guided by the nature of the carboxylate anions, which allows an effective tuning of the self-aggregate process within same ligand environment. The study of the magnetic properties reveals that **1** exhibits an $S = 3$ ground state. Nevertheless, the magnetization increases above the expected saturation value of 6 μ_B at higher fields, because of the suppression of antiferromagnetic exchange between the central and peripheral Ni(II) ions. Complexes **2** and **3** exhibit ferromagnetic exchange interactions that result in the $S = 4$ ground state. Examination of AC magnetic susceptibility showed that complex **2** in finely ground form behaves as spin glass with the spin-freezing temperature of ~5.5 K. This behavior was attributed to the collapse of the structure upon the loss of interstitial solvent. Such property was not observed for complex **3**, in which the bulkier carboxylate ligands provide for a more robust crystal packing and larger separation between the $[Ni_4O_4]$ clusters.

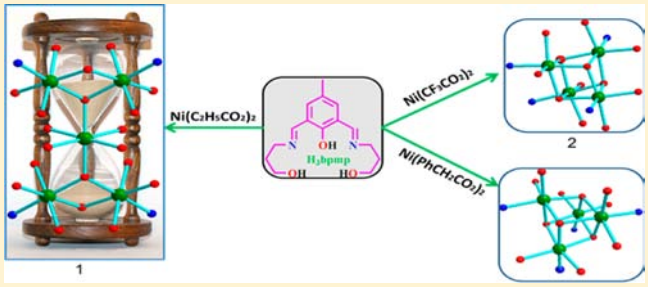

INTRODUCTION

Synthesis and characterization of multinuclear coordination cluster complexes of 3d metal ions have become of particular interest in recent times because of their relevance to bioinorganic chemistry and to new magnetic materials.[1] A number of magnetic cluster complexes behave as single-molecule magnets (SMMs) because of the combination of large ground-state spin (S) with a large Ising (or easy-axis) type magnetic anisotropy that stems from a negative and axial zero-field-splitting parameter (D).[2] Self-aggregation of transition metal ions is mostly achieved by oxygen-containing bridges, such as hydroxide, oxide, phenolate, and carboxylate. The nature of the coordinating ligands plays the most crucial role for the formation of the products. The rational assembly of component small molecules into larger supramolecular cluster complexes thus continues to be a major theme in modern synthetic transition metal chemistry.

Thus, there is a clear demand for new synthetic approaches to multinuclear metal complexes which can show promise for high-spin or SMM behavior.[3] The choice of ligands is always a major issue in the development of new synthetic routes to this type of coordinations clusters.[4] Phenol-centered "dinucleating ligands", known during last 40 years,[5] are able to bind simultaneously two metal ions. Bearing two adjacent imine arms, these ligands can provide M_2L type complexes[6] in absence of other supporting bridges. Introduction of secondary bridging units, such as HO^- or O^{2-}, from deprotonation of solvent water molecules[7,8] can result

Received: May 28, 2013
Published: December 2, 2013

   dx.doi.org/10.1021/ic401337q | Inorg. Chem. 2013, 52, 13894−13903

in the assembly of transition metal coordination clusters from two or more M_2L units.[7,8] Such clusters display a variety of topologies, for example, tetrahedron,[7] cubane,[9a−c] open dicubane,[10] fused defective open dicubane,[11a,b] pentanuclear vertex-shared double cubane (hourglass),[12] and stepped cubane[13] (Scheme 1).

Scheme 1. Growth of Penta- and Tetranuclear Nickel Assemblies Depending on the Primary and Supporting Ligands

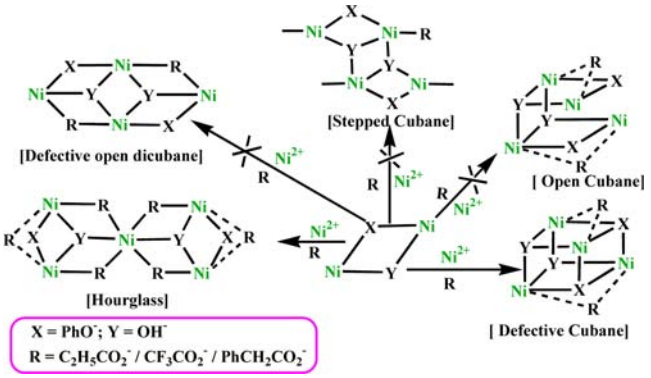

Among the ancillary ligands used, hydroxide and carboxylate groups offer versatile bridging modes (Supporting Information Scheme S2). One hydroxide group can bridge two to six metal ions in the assembly reaction.[14,15] Both aliphatic and aromatic carboxylate groups can adopt numerous coordination modes such as terminal, chelating, bridging syn−anti in μ-1,1 mode (Supporting Information Scheme S2a−c), syn−syn, syn−anti, and anti−anti in μ-1,3 mode (Supporting Information Scheme S2d−h), anti−syn−syn and anti−syn−anti in μ_3-1,1,3 mode- (Supporting Information Scheme S2i,j), and syn−anti−syn−anti in μ_4-1,1,3,3 mode (Supporting Information Scheme S2k) satisfying the coordination requirement and charge demand of the transition metal ions (Supporting Information Scheme S2).[16]

Scheme 2. Bridging Mode of Hydroxide and Carboxylate Anions

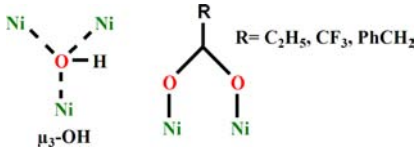

In trying to prepare and study new forms of $[Ni_5]$ and $[Ni_4]$ aggregates from the assembly of ligated $[Ni_2]$ basic units, we have been interested in exploring the reactivity of 2,6-*bis*-[(2-hydroxypropylimino)-methyl]-4-methylphenol (H_3bpmp, Chart 1)[17] with three $Ni(RCO_2)_2{\cdot}4H_2O$ salts (R = C_2H_5, CF_3, $PhCH_2$) in presence of NEt_3. It is worth noting that the use of a closely related ligand, H_3bemp (Chart 1, right, 2,6-bis-[(2-hydroxy-ethylimino)-methyl]-4-methylphenol), led to exciting $[Ni_6]$[18] and $[Ni_6, Ni_4]$[13] clusters.

Chart 1. H_3bpmp and H_3bemp

Herein, we report the synthesis of three new Ni(II) complexes with the H_2bpmp^- anionic ligand: the pentanuclear vertex shared dicubane complex **1**·2H_2O·4DMF and tetranuclear cubane complexes **2**·H_2O and **3**·4H_2O, both containing two μ_3-phenoxide and two μ_3-hydroxide anions at the corners of the cubane. The crystal structures and magnetic properties of these complexes are also described and discussed.

EXPERIMENTAL SECTION

Materials. $Ni(C_2H_5CO_2)_2{\cdot}4H_2O$, $Ni(CF_3CO_2)_2{\cdot}4H_2O$, and $Ni(PhCH_2CO_2)_2{\cdot}4H_2O$ were synthesized by adding nickel(II) carbonate (60 mg) to a solution of propanoic acid, trifluoroacetic acid, and phenylacetic acid each (74.08, 114.02, 136.15 mg, respectively) in 30 mL of water under constant glass-rod stirring until effervescence had stopped. Then the solution was filtered, and the clear filtrate was kept over a water bath until a solid started to precipitate. The solution was then cooled to room temperature, and the solid was filtered through suction and dried in vacuum. The chemicals used were obtained from the following sources: nickel(II) carbonate from Universal Laboratory (India), trifluoroacetic acid, propanoic acid, phenyl acetic acid, triethylamine from E. Merck (India), and 3-amino-1-propanol from Aldrich Chemical Co. Inc. (U.S.). These chemicals and solvents were reagent-grade materials and were used as received without further purification. 2,6-Diformyl-4-methylphenol (2-hydroxy-5-methyl-benzene-1,3-dicarbaldehyde) was prepared following a literature procedure.[19] All manipulations were performed under aerobic conditions.

Syntheses. *H_3bpmp Ligand.* The H_3bpmp Schiff-base ligand was prepared from the single-step condensation of 2,6-diformyl-4-methylphenol (1.0 g, 6.1 mmol) and 3-amino-1-propanol (0.91 g, 12.2 mmol) in methanol (20 mL) in air at room temperature (28 °C) under stirring for 2 h following a reported procedure.[17] Complete evaporation of solvent in air for 12 h yielded an orange-colored semisolid product, which was used directly for reactions with metal salts. Because of its semisolid nature, the ligand obtained from this reaction was not of excellent purity. CHN analysis was more or less close to the theoretical values and major proton NMR signals were also characteristic indication the Schiff base condensation at two arms of the ligand. Yield: 1.32 g (78%).

*$[Ni_5(\mu_3\text{-}OH)_2(\mu\text{-}H_2bpmp)_2(\mu_{1,3}\text{-}O_2CC_2H_5)_6]{\cdot}2H_2O{\cdot}4DMF$ (**1**·2H_2O·4DMF).* $Ni(C_2H_5CO_2)_2{\cdot}4H_2O$ (0.691 g, 2.50 mmol) dissolved in MeOH (20 mL) was added dropwise to a yellow MeOH solution (10 mL) of H_3bpmp (0.278 g, 1.00 mmol) followed by dropwise addition of NEt_3 (0.278 mL, 0.202 g, 2.00 mmol) during 5 min. The green solution was next stirred for 2.5 h at room temperature. The solvent was evaporated in air to give a green solid, which was isolated, washed with cold methanol and dried under vacuum over P_4O_{10}. Green crystals suitable for single crystal X-ray analysis were obtained from a saturated DMF solution after three weeks. Yield (green solid): 0.601 g, 73%. Anal. Calcd. for $C_{60}H_{106}Ni_5N_8O_{26}$ (1649.05 g mol^{-1}): C, 43.70; H, 6.47; N, 6.79. Found: C, 43.77; H, 6.42; N, 6.84. Selected FT-IR bands: (KBr, cm^{-1}; s = strong, vs = very strong, m = medium, br = broad) 3399(br), 2930(s), 2367(m), 1637(s), 1570(vs), 1459(s), 1409(s), 1384(vs), 1074(s), 764(s), 626(s). Molar conductance, Λ_M: (DMF solution) 3.4 Ω^{-1} cm^2 mol^{-1}. UV−vis spectra [λ_{max}, nm (ε, L mol^{-1} cm^{-1})]: (MeOH solution) 663 (725), 371 (1289), 258 (51237).

*Compounds $[Ni_4(\mu_3\text{-}OH)_2(\mu_3\text{-}H_2bpmp)_2(\mu_{1,3}\text{-}O_2CCF_3)_2](CF_3CO_2)_2{\cdot}H_2O$ (**2**·H_2O) and $[Ni_4(\mu_3\text{-}OH)_2(\mu_3\text{-}H_2bpmp)_2(\mu_{1,3}\text{-}O_2CCH_2Ph)_2](PhCH_2CO_2)_2{\cdot}4H_2O$ (**3**·4H_2O).* **2**·H_2O and **3**·4H_2O were obtained following the same procedure as outlined above for the synthesis of **1** by using $Ni(CF_3CO_2)_2{\cdot}4H_2O$ and $Ni(PhCH_2CO_2)_2{\cdot}4H_2O$ in place of $Ni(C_2H_5CO_2)_2{\cdot}4H_2O$. The obtained yields were 77% and 71%, respectively, for **2** and **3**. For **2**, Anal. Calcd for $C_{38}H_{46}Ni_4N_4O_{17}F_{12}$ (1293.63g mol^{-1}): C, 35.28; H, 3.58; N, 4.33. Found: C, 34.47; H, 3.68; N, 4.39. Selected FT-IR bands: (KBr, cm^{-1}) 3409(br), 2925(m), 1668(vs), 1568(s), 1451(m), 1311(m), 1202(s), 1137(m), 1074(m),

dx.doi.org/10.1021/ic401337q | Inorg. Chem. 2013, 52, 13894−13903

Table 1. Crystallographic Data for $1{\cdot}2H_2O{\cdot}4DMF$, $2{\cdot}H_2O$, and $3{\cdot}4H_2O$

compound	$1{\cdot}2H_2O{\cdot}4DMF$	$2{\cdot}H_2O$	$3{\cdot}4H_2O$
formula	$C_{60}H_{106}Ni_5N_8O_{26}$	$C_{38}H_{46}F_{12}N_4Ni_4O_{17}$	$C_{62}H_{80}Ni_4N_4O_{20}$
M	1649.08	1293.63	1436.14
space group	$P2_1/n$	$P2_1/c$	$P2_1$
crystal system	monoclinic	monoclinic	monoclinic
a (Å)	11.8638(8)	17.896(1)	11.0227(1)
b (Å)	16.560(1)	14.122(1)	18.6158(3)
c (Å)	19.494(1)	20.306(2)	16.4947(3)
β (deg)	90.990(3)	97.953(2)	94.6647(6)
V (Å^3)	3829.8(5)	5082.6(6)	3373.44(9)
T (K)	295	295	295
Z	2	4	2
D_c (g cm^{-3})	1.430	1.691	1.414
$F(000)$	1732	2656	1504
crystal size (mm)	0.38 × 0.27 × 0.18	0.41 × 0.29 × 0.17	0.42 × 0.34 × 0.31
μ(Mo Kα) (cm^{-1})	12.85	15.74	11.72
measured reflns	49815	52719	24480
unique reflns	8295	8866	8234
R_{int}	0.0461	0.0652	0.0389
obs. reflns [$I \geq 2\sigma(I)$]	5903	6378	7207
θ_{min}–θ_{max} (deg)	1.61–27.00	1.17–25.00	2.56–27.90
hkl ranges	−14, 14; −21, 21; −24, 24	−21, 21; −16, 16; −23, 24	−14, 14; −22, 24; −20, 21
R1(F^2)[a] (obs. reflns)	0.0485	0.0853	0.0372
wR2(F^2)[a] (all reflns)	0.1455	0.1950	0.0460
no. variables	452	700	735
goodness of fit	1.016	1.170	1.060
$\Delta\rho_{max}$, $\Delta\rho_{min}$ (e Å^{-3})	0.69, −0.52	1.43, −0.68	0.72, −0.47

[a] $R1 = \Sigma(||F_o| - |F_c||)/\Sigma|F_o|$. $wR2 = [\Sigma w(|F_o| - |F_c|)^2/\Sigma w(F_o)^2]^{1/2}$. $w = 0.75/(\sigma^2(F_o) + 0.0010F_o^2)$.

928(m), 846(m), 729(m). Molar conductance, Λ_M: (MeOH solution) 142 Ω^{-1} cm^2 mol^{-1}. UV–vis spectra, [λ_{max}, nm (ε, L mol^{-1} cm^{-1})]: (MeOH solution) 673 (396), 373(1476), 258(70737). For **3**, Anal. Calcd for $C_{62}H_{80}Ni_4N_4O_{20}$ (1436.14 g mol^{-1}): C, 51.85; H, 5.61; N, 3.90. Found: C, 51.87; H, 5.72; N, 3.96. Selected FT-IR bands: (KBr, cm^{-1}) 3366(br), 2910(s), 1636(s), 1576(vs), 1388(vs), 1311(m), 1075(s), 930(m), 805(m), 706(m), Molar conductance, Λ_M: (DMF solution) 155 Ω^{-1} cm^2 mol^{-1}. UV–vis spectra [λ_{max}, nm (ε, L mol^{-1} cm^{-1})]: (MeOH solution) 676 (322), 370 (8563), 261 (69120).

Physical Measurements. The elemental analyses (C, H, N) were performed with a Perkin-Elmer model 240 C elemental analyzer. Fourier transform infrared (FT-IR) spectra were recorded on a Perkin-Elmer RX1 spectrometer. Solution electrical conductivity measurements and electronic spectra were carried out using a Unitech type U131C digital conductivity meter with a solute concentration of about 10^{-3} M and a Shimadzu UV 3100 UV–vis–NIR spectrophotometer, respectively.

Magnetic Measurements. Magnetic measurements were performed on microcrystalline samples of $1{\cdot}2H_2O{\cdot}4DMF$, $2{\cdot}H_2O$, and $3{\cdot}4H_2O$, using a Quantum Design SQUID magnetometer MPMS-XL. DC magnetic susceptibility was measured in an applied field of 0.1 T, in the 1.8–300 K temperature range. Isothermal dependences of magnetization were measured at 1.8 K with the magnetic field varying from 0 to 7 T. AC magnetic susceptibility was measured under zero DC bias field, in the 1.8–50 K range, with the AC field amplitude of 0.5 mT and frequencies of 1, 10, 100, and 1000 Hz. The data were corrected for diamagnetic contributions using tabulated constants.[20]

X-ray Crystallography. Single-crystal X-ray diffraction data of $1{\cdot}2H_2O{\cdot}4DMF$ and $2{\cdot}H_2O$ were collected on a Bruker-APEX-2 CCD X-ray diffractometer using graphite-monochromated Mo Kα radiation (λ = 0.7107 Å) by ω-scan at 293 K. The data for $3{\cdot}4H_2O$ were collected at room temperature using a Nonius Kappa CCD diffractometer. All the data sets were integrated with the Denzo-SMN package[21] and corrected for Lorentz, polarization, and absorption effects (SORTAV[22]). The structures were solved by direct methods (SIR97[23]) and refined using full-matrix least-squares with anisotropic atomic displacement parameters for all non-hydrogen atoms. Hydrogen atoms were included on calculated positions, riding on their carrier atoms. All the calculations were performed using SHELXL-97[24] and PARST[25] implemented in WINGX suite of programs.[26] Information concerning X-ray data collection and crystal structure refinement is summarized in Table 1. Crystallographic data (excluding structure factors) have been deposited with the Cambridge Crystallographic Data Centre as supplementary publications CCDC-869973, 878614, and 878615. These data can be obtained free of charge at www.ccdc.cam.ac.uk/conts/retrieving.html (or from the Cambridge Crystallographic Data Centre, 12, Union Road, Cambridge CB2 1EZ, U.K.; fax +44–1223/336–033; e-mail deposit@ccdc.cam.ac.uk).

RESULTS AND DISCUSSION

Synthetic Considerations. The Schiff-base ligand 2,6-bis-[(3-hydroxy-propylimino)-methyl]-4-methylphenol (H_3bpmp) was prepared following a literature procedure (Scheme S1 in the Supporting Information),[17] and its reactions with three nickel(II) salts have been systematically investigated to explore the roles of different carboxylate anions for cluster assembly as summarized in Supporting Information Scheme S3. Two types of self-assembly processes involving ligand bound [Ni_2] fragments were responsible for the formation of the products. A variety of reactions were explored with different solvents and under different reagent ratios before the following successful procedures were identified. The reaction of $Ni(C_2H_5CO_2)_2{\cdot}4H_2O$, H_3bpmp, and NEt_3 in a 5:2:4 ratio in MeOH afforded a greenish solution, from which was subsequently isolated **1** as green solid in 73% yield. Variations in the reaction stoichiometry also gave product **1** but in lower yield. The formation of **1** is summarized by eq 1, which also accounts for the formation of hydroxido bridges from the water molecules present in the solvent system used. Crystals of $1{\cdot}2H_2O{\cdot}4DMF$ were obtained from a DMF solution.

dx.doi.org/10.1021/ic401337q | Inorg. Chem. 2013, 52, 13894–13903

$$2H_3bpmp + 5Ni(C_2H_5CO_2)_2\cdot 4H_2O + 4NEt_3 \rightarrow [Ni_5(\mu\text{-}H_2bpmp)_2(\mu_3\text{-}OH)_2(\mu_{1,3}\text{-}O_2CC_2H_5)_6] + 4(HNEt_3)(C_2H_5CO_2) + 18H_2O \quad (1)$$

The elemental analysis, molar conductivity data and single-crystal X-ray diffraction support the composition $[Ni_5(\mu\text{-}H_2bpmp)_2(\mu_3\text{-}OH)_2(\mu_{1,3}\text{-}O_2CC_2H_5)_6]\cdot 2H_2O\cdot 4DMF$ (**1**·2H_2O·4DMF).

To identify the role of ancillary carboxylate ligands for the self-aggregation, the above stated reaction (eq 1) was repeated with $Ni(CF_3CO_2)_2\cdot 4H_2O$ in place of $Ni(C_2H_5CO_2)_2\cdot 4H_2O$. The reaction of $Ni(CF_3CO_2)_2\cdot 4H_2O$, H_3bpmp, and NEt_3 in a 4:2:4 ratio in MeOH provided **2** as green solid in 77% yield:

$$2H_3bpmp + 4Ni(CF_3CO_2)_2\cdot 4H_2O + 4NEt_3 \rightarrow [Ni_4(\mu_3\text{-}H_2bpmp)_2(\mu_3\text{-}OH)_2(\mu_{1,3}\text{-}O_2CCF_3)_2](CF_3CO_2)_2 + 4(HNEt_3)(CF_3CO_2) + 12H_2O \quad (2)$$

The elemental analysis, molar conductivity data and single-crystal X-ray structure confirm the formula $[Ni_4(\mu_3\text{-}H_2bpmp)_2(\mu_3\text{-}OH)_2(\mu_{1,3}\text{-}O_2CCF_3)_2](CF_3CO_2)_2\cdot H_2O$ (**2**·H_2O).

To further explore the role of the carboxylate ligand on the cluster formation, a reaction of $Ni(PhCH_2CO_2)_2\cdot 4H_2O$, H_3bpmp, and NEt_3 in 4:2:4 ratio in MeOH was performed to provide **3** as slightly dark-green solid in 71% yield. The preparative route to **3** is summarized in eq 3 establishing once again the importance of anionic parts available from the precursor metal salts in the outcome of the reaction.

$$2H_3bpmp + 4Ni(PhCH_2CO_2)_2\cdot 4H_2O + 4NEt_3 \rightarrow [Ni_4(\mu_3\text{-}H_2bpmp)_2(\mu_3\text{-}OH)_2(\mu_{1,3}\text{-}O_2CCH_2Ph)_2](PhCH_2CO_2)_2\cdot 4H_2O + 4(HNEt_3)(PhCH_2CO_2) + 10H_2O \quad (3)$$

The elemental analysis, molar conductivity, and X-ray diffraction data establish the formula of the product as $[Ni_4(\mu_3\text{-}H_2bpmp)_2(\mu_3\text{-}OH)_2(\mu_{1,3}\text{-}O_2CCH_2Ph)_2](PhCH_2CO_2)_2\cdot 4H_2O$ **3**·4H_2O, containing free carboxylate counterions. Thus, the use of phenyl tail bearing carboxylate ligand did not change the mode of aggregation toward a different nuclearity as compared to the reaction carried out with trifluoroacetate. Both **2** and **3** contain a face-capped cubic $[Ni_4]$ structure supported by endogenous μ_3-phenoxide and exogenous μ_3-hydroxide ligands. During the formation of these clusters, equally probable solvent derived μ_3-OMe bridging groups were not trapped in place of μ_3-OH groups.[27] Basicity differences of the used carboxylates guided the aggregation of the $[Ni_2]$ building motifs. When R = Et, more carboxylates (six altogether) bind to the Ni ions compared to the cases where R = CF_3 and $PhCH_2$.

FT-IR Spectra. The presence of nickel-bound terminal and bridging HO^- groups and interstitial water molecules in **1**·2H_2O·4DMF, **2**·H_2O, and **3**·4H_2O is manifested by a broad and medium intensity bands at 3399, 3409, and 3366 cm^{-1}, respectively, assignable to $\bar{\nu}_{OH}$ stretching frequencies. Extensive hydrogen bonding leads to band broadening and shift to lower frequencies. The $\bar{\nu}_{C=N}$ stretching frequencies are observed within 1636–1668 cm^{-1} for the three complexes. Analysis of carboxylate stretching frequencies allowed us to identify the mode of their binding as observed by X-ray crystal structure determinations (vide infra).[28] The strong asymmetric $\bar{\nu}_{as(COO)}$ vibration for **1** is observed at 1570 cm^{-1} and the symmetric $\bar{\nu}_{s(COO)}$ vibration is found at 1384 cm^{-1}. The difference, $\Delta\bar{\nu} = \bar{\nu}_{as(COO)} - \bar{\nu}_{s(COO)}$ = 186 cm^{-1}, is indicative of $\mu_{1,3}$-bridging propionates. For **2** and **3** the corresponding values for trifluoroacetate and phenylacetate groups are 1568 and 1576 cm^{-1} ($\bar{\nu}_{as(COO)}$) and 1311 and 1388 cm^{-1} ($\bar{\nu}_{s(COO)}$), resulting in $\Delta\bar{\nu}$ values of 257 and 188 cm^{-1}, resepectively.[29,30] For nonbridging carboxylato coordination, this $\Delta\bar{\nu}$ separation is usually larger (~350 cm^{-1}).[8]

Electronic Spectra. Moderate solubility of all three complexes in MeOH allowed spectroscopic characterizations by recording optical absorption spectra in the 200–900 nm regions. Broad absorption bands with maxima at 663 (ε = 725 L mol^{-1} cm^{-1}), 673 (ε = 147 L mol^{-1} cm^{-1}), and 676 nm (ε = 322 L mol^{-1} cm^{-1}) for **1**, **2**, and **3**, respectively, can be assigned to the spin-allowed $^3A_{2g}(F) \rightarrow {}^3T_{1g}(F)$ transition of Ni(II) ion in the slightly distorted octahedral coordination. The lower energy $^3A_{2g}(F) \rightarrow {}^3T_{2g}(F)$ transition was not observed in the accessible wavelength range.[31] The $^3A_{2g}(F) \rightarrow {}^3T_{1g}(P)$ transition appears at 371 nm (ε = 1289 L mol^{-1} cm^{-1}), 373 nm (ε = 1476 L mol^{-1} cm^{-1}) and 370 nm (ε = 8563 L mol^{-1} cm^{-1}) for **1**, **2** and **3**, respectively.[32] The intense absorptions at 258 (ε = 51237 L mol^{-1} cm^{-1}), 259 (ε = 70737 L mol^{-1} cm^{-1}), and 261 nm (ε = 169120 L mol^{-1} cm^{-1}) are because of ligand-centered $\pi \rightarrow \pi^*$ transitions.

Description of Structures. *$[Ni_5(\mu\text{-}H_2bpmp)_2(\mu_3\text{-}OH)_2(\mu_{1,3}\text{-}O_2CC_2H_5)_6]\cdot 2H_2O\cdot 4DMF$ (**1**·2H_2O·4DMF).* The molecular structure of **1** is shown in Figure 1, and selected interatomic distances

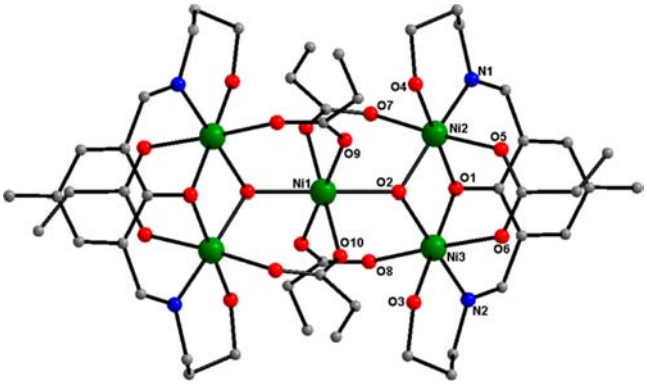

Figure 1. Partially labeled plot of $[Ni_5]$ cluster of **1**. Symmetry equivalent atoms are not labeled. Color scheme: Ni, green; O, red; N, blue; C, gray.

and angles are listed in Table 2. Single-crystal X-ray diffraction revealed that the compound crystallizes in the monoclinic space group $P2_1/n$. The molecule of **1** consists of five Ni^{II} ions held together by two doubly bridging phenoxido groups (μ-O1 and its symmetry equivalent, s.e.), two triply bridging hydroxido groups (μ_3-O2 and its s.e.), four *syn,syn*-$\eta^1{:}\eta^1{:}\mu$-$C_2H_5CO_2^-$ groups of one type (O7 to O10 and their s.e.), and two of the other type (O5, O6 and their s.e.). Peripheral ligation is provided by two monodeprotonated $Hbpmp^-$ ligands (N1, N2, O3, O4, and their s.e.). The coordination modes of the bridging ligands present in **1** are shown in Supporting Information Scheme S4. The five Ni^{II} ions are disposed in a centered parallelogram. Alternatively the cluster topology can be considered as two Ni^{II} triangles (Ni1–Ni2–Ni3 and Ni1–Ni2′–Ni3′) with a common vertex on Ni1. Each triangle is nearly isosceles, spanned by six carboxylate

dx.doi.org/10.1021/ic401337q | Inorg. Chem. 2013, 52, 13894–13903

Table 2. Selected Interatomic Distances (Å) and Angles (deg) for 1·2H$_2$O·4DMF

distances			
O5−Ni2	2.043(2)	Ni2−O1	2.027(2)
O7−Ni2	2.041(2)	Ni2−N1	2.048(3)
O8−Ni3	2.035(3)	Ni2−O2	2.068(2)
O10−Ni1	2.103(2)	Ni2−O4	2.068(3)
O9−Ni1	2.062(3	Ni2···Ni3	2.9713(6)
Ni1−O2^a	2.033(2)	Ni3−N2	2.022(3)
Ni1−O2	2.033(2)	Ni3−O2	2.032(2)
Ni1−O9^a	2.062(3)	Ni3−O1	2.059(2)
Ni1−O10^a	2.103(2)	Ni3−O3	2.094(3)
angles			
O2^a−Ni1−O2	180.00	O7−Ni2−O4	91.2(1)
O2−Ni1−O9	95.1(1)	O1−Ni2−Ni3	43.79(7)
O2^a−Ni1−O9	84.9(1)	N1−Ni2−Ni3	133.55(9)
O2−Ni1−O9^a	84.9(1)	O2−Ni2−Ni3	43.17(7)
O2^a−Ni1−O9^a	95.1(1)	O7−Ni2−Ni3	103.52(8)
O9^a−Ni1−O9	180.0	O5−Ni2−Ni3	79.83(8)
O2−Ni1−O10	92.6(1)	O4−Ni2−Ni3	133.28(7)
O2^a−Ni1−O10	86.4(1)	N2−Ni3−O2	176.7(1)
O9^a−Ni1−O10^a	94.2(1)	N2−Ni3−O1	91.3(1)
O9−Ni1−O10^a	85.8(1)	O2−Ni3−O1	85.75(9)
O2−Ni1−O10^a	86.4(1)	N2−Ni3−O8	85.9(1)
O2−Ni1−O10	93.6(1)	O2−Ni3−O8	92.9(1)
O9^a−Ni1−O10	86.8(1)	O1−Ni3−O8	92.5(1)
O9−Ni1−O10	94.2(1)	N2−Ni3−O3	92.8(1)
O10−Ni1−O10	180.00	O2−Ni3−O3	90.2(1)
O1−Ni2−N1	90.9(1)	O1−Ni3−O3	174.1(1)
O1−Ni2−O2	85.74(9)	O8−Ni3−O3	92.1(1)
N1−Ni2−O2	176.6(1)	N2−Ni3−O6	90.7(1)
O1−Ni2−O7	93.7(1)	O2−Ni3−O6	90.5(1)
N1−Ni2−O7	85.6(1)	O1−Ni3−O6	87.3(1)
O2−Ni2−O7	94.25(9)	O8−Ni3−O6	176.6(1)
O1−Ni2−O5	87.6(1)	O3−Ni3−O6	88.4(1)
N1−Ni2−O5	90.8(1)	N2−Ni3−Ni2	133.3(1)
O2−Ni2−O5	89.3(1)	O2−Ni3−Ni2	44.04(6)
O7−Ni2−O5	176.3(1)	O1−Ni3−Ni2	42.93(6)
O1−Ni2−O4	173.2(1)	O8−Ni3−Ni2	101.69(9)
N1−Ni2−O4	94.2(1)	O3−Ni3−Ni2	132.16(8)
O2−Ni2−O4	89.3(1)	O6−Ni3−Ni2	80.43(8)

^{a}Symmetry operations used to generate equivalent atoms: $-x$, $1-y$, $-z$.

bridges with two longer Ni···Ni separations of 3.608 and 3.617 Å and one shorter separation of 2.951 Å (Figure 2). Each of the four triatomic carboxylate groups bridges the central Ni^{II} ion and one peripheral Ni^{II} ion. The remaining two carboxylate groups complete the triply bridging motif between Ni2 and Ni3. The μ_3-HO$^-$ group links the central Ni^{II} ion with the peripheral metal

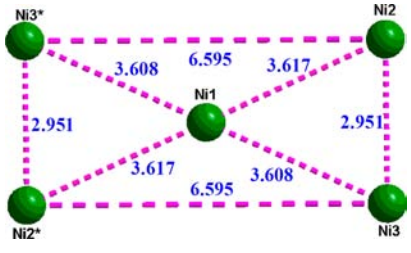

Figure 2. Ni$_5$ skeleton of **1** showing centered rectangular topology of the internuclear distances (Å).

ions on either side of the molecule. The formation of the cluster can be considered as the result of entrapment of the central Ni^{II} ion (from the salt Ni(C$_2$H$_5$CO$_2$)$_2$·4H$_2$O) by two dinuclear [Ni$_2$(μ-H$_2$bpmp)] units.

The μ_3-O2 donor atom lies 0.500 Å out of the plane of the three connected Ni^{II} ions: the solid angle around this atom is 341.6° and two of the Ni−O−Ni angles are significantly larger (124.3° and 124.7° for the angles subtended at the central Ni^{II} ion) than the third one (92.7° for the angle derived to the peripheral Ni^{II} ions) (Supporting Information Figure S1). The core of the molecule is {Ni$_5$(μ-OPh)$_2$(μ-OH)$_2$}$^{6+}$ (Figure 3,

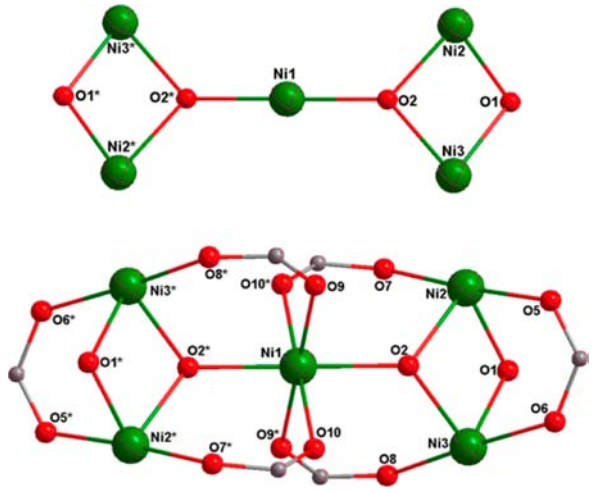

Figure 3. {Ni$_5$(μ-OPh)$_2$(μ-OH)$_2$}$^{6+}$ core of **1** (top) and a more detailed representation emphasizing its {Ni$_5$(μ_3-OH)$_2$(μ_2-OPh)$_2$($\mu_{1,3}$-OCC$_2$H$_5$)$_6$} description (bottom). Color code: Ni, dark green; O, red; N, blue; C, gray.

top). This Ni$_5$ fragment or its trinuclear Ni$_3$ subfragment is common to other Ni^{II} cluster complexes..[33] If we consider all six propanoate bridges as part of the linking groups, then the metallic core becomes {Ni$_5$(μ-OPh)$_2$(μ-OH)$_2$(μ-O$_2$CC$_2$H$_5$)$_6$} (Figure 3, top). The μ-C$_2$H$_5$CO$_2^-$ groups bridge Ni^{II} ions in similar modes but twisting within the O−C−O planes leads to six different Ni−O bond distances within 2.05−2.09 Å range (Supporting Information Figure S2). Terminal Ni2 and Ni3 atoms are bound to an O$_5$N set of donor atoms in H$_2$bpmp$^-$ ligand environment, while Ni1 remains in H$_2$bpmp-free symmetric O$_6$ environment with Ni−O bond distances within 2.038−2.092 Å range, having tetragonal elongation along the axis defined by the propionate O9 and O9* atoms (Supporting Information Figure S3). Thus, all of the Ni^{II} atoms are six-coordinate with distorted octahedral geometry (Supporting Information Figure S4).

The crystal structure of **1**·2H$_2$O·4DMF is stabilized by two O(propanoate)···O(lattice H$_2$O) hydrogen bonds at 3.005 Å and O(DMF)···O(lattice H$_2$O) hydrogen bonds from the other side at 2.824 Å. The coordinated ligand alcohol arms bearing (H)O3 and (H)O4 are hydrogen bonded to propionate O10 and O9 atoms with O···O separations of 2.646 and 2.757 Å, respectively (Supporting Information Figures S5 and S6).

[Ni$_4$(μ_3-OH)$_2$(μ_3-H$_2$bpmp)$_2$($\mu_{1,3}$-O$_2$CCF$_3$)$_2$](CF$_3$CO$_2$)$_2$·H$_2$O (***2***·*H$_2$O*) *and [Ni$_4$(μ_3-H$_2$bpmp)$_2$(μ_3-OH)$_2$($\mu_{1,3}$-O$_2$CCH$_2$Ph)$_2$]-(PhCH$_2$CO$_2$)$_2$·4H$_2$O* (***3***·*4H$_2$O*). The molecular structures of **2**·H$_2$O and **3**·4H$_2$O are shown in Figure 4. Selected interatomic distances and angles are provided in Tables 3 and 4 and Supporting Information Table S1. Single-crystal X-ray diffraction

dx.doi.org/10.1021/ic401337q | Inorg. Chem. 2013, 52, 13894−13903

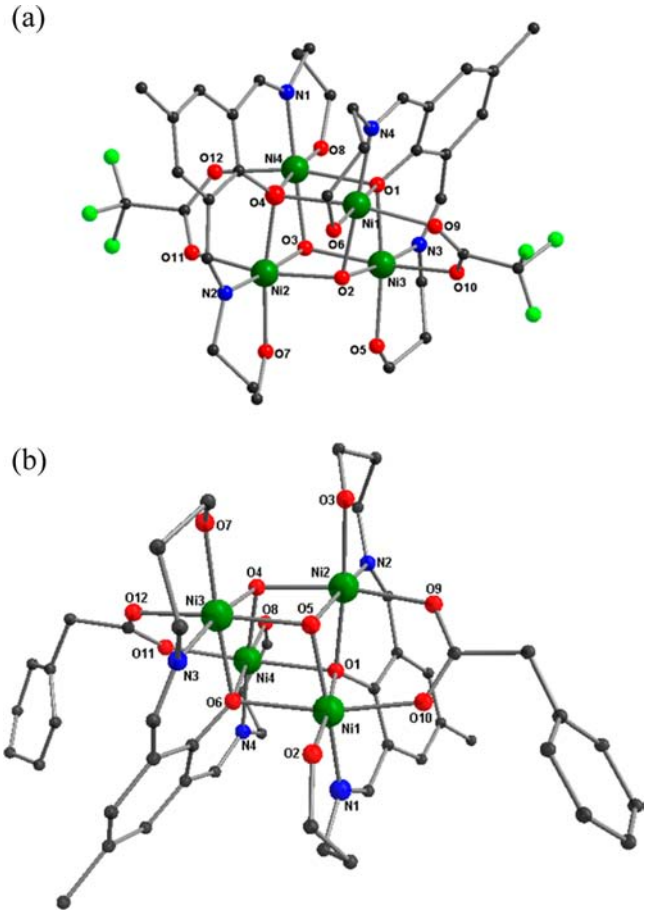

Figure 4. Partially labeled molecular structures of Ni_4 cationic clusters in **2**·H_2O (a) and **3**·$4H_2O$ (b). Color scheme: Ni, dark green; O, red; N, blue; C, black; F, light green.

revealed that these compounds crystallize in monoclinic space groups $P2_1/c$ and $P2_1$, respectively. Eight alternately arranged oxygen and metal atoms form two distorted $\{Ni_4O_4\}$ cubes with local S_4-symmetry. In case of complex **2**·H_2O the structure consists of a dicationic tetrametallic part $[Ni_4(\mu_3\text{-}OH)_2(\mu_3\text{-}H_2bpmp)_2(\mu_{1,3}\text{-}O_2CCF_3)_2]^{2+}$ and two $CF_3CO_2^-$ anions.

In **3**·$4H_2O$ the cluster fragment $[Ni_4(\mu_3\text{-}OH)_2(\mu_3\text{-}H_2bpmp)_2(\mu_{1,3}\text{-}O_2CCH_2Ph)_2]^{2+}$ is cocrystallized with two $PhCH_2CO_2^-$ anions. The carboxylate groups serve a dual role of bridging the metal ions and stabilizing crystal packing through multiple hydrogen bonding interactions. All the Ni ions are six-coordinate, with a distorted O_5N octahedral coordination (Figure 5 and Supporting Information Figure S7). Three corners of the octahedron are occupied either by two O atoms from the phenoxide and one O atom from hydroxide donor or by one O atom from the phenoxide and two O atoms from hydroxide donors, which act as bridges to the remaining metal ions within the cubane core. Remaining positions are occupied by an O atom from the propanol OH arm, the imine-N atom of the H_2bpmp ligand and one O atom of the exogenous carboxylate anion. Bridge extending capabilities of hydroxide and phenoxide groups are crucial for the condensation of two dinuclear $[Ni_2]$ fragments without any reorganization of the coordination spheres of the Ni^{II} ions. The bound carboxylate groups (O9, O10, O11, and O12 for **2**·$2H_2O$ and O10, O9 and O12, O11 for **3**·$4H_2O$) push the individual $[Ni_2]$ units to each other to establish new Ni–O bonds from opposite sides. Both clusters are based on cubic

Table 3. Selected Interatomic Distances (Å) for 2·H_2O and 3·$4H_2O$

2·H_2O			
Ni1–O2	2.009(5)	Ni2···Ni4	2.962(1)
Ni1–N4	2.032(6)	Ni3–N3	2.012(7)
Ni1–O6	2.047(6)	Ni3–O2	2.023(5)
Ni1–O9	2.059(5)	Ni3–O3	2.037(5)
Ni1–O1	2.070(5)	Ni3–O1	2.072(5)
Ni1–O4	2.199(5)	Ni3–O5	2.085(6)
Ni1···N3	2.979(1)	Ni3–O10	2.147(5)
Ni2–N2	2.008(7)	Ni4–O3	2.016(5)
Ni2–O3	2.012(6)	Ni4–O8	2.027(6)
Ni2–O2	2.055(5)	Ni4–N1	2.032(7)
Ni2–O4	2.074(5)	Ni4–O4	2.063(5)
Ni2–O7	2.091(5)	Ni4–O12	2.079(6)
Ni2–O11	2.095(5)	Ni4–O1	2.211(5)
3·$4H_2O$			
Ni1–O5	1.990(3)	Ni3–O4	2.020(3)
Ni1–N1	2.015(4)	Ni3–O5	2.024(3)
Ni1–O10	2.027(4)	Ni3–N3	2.028(4)
Ni1–O2	2.048(3)	Ni3–O7	2.050(4)
Ni1–O1	2.072(3)	Ni3–O6	2.086(3)
Ni1–O6	2.223(3)	Ni3–O12	2.092(4)
Ni1···Ni2	2.9370(7)	Ni3···Ni4	2.9439(7)
Ni2–O5	2.022(3)	Ni4–O4	1.989(3)
Ni2–N2	2.042(4)	Ni4–N4	2.030(4)
Ni2–O3	2.044(3)	Ni4–O11	2.049(4)
Ni2–O4	2.048(3)	Ni4–O8	2.053(3)
Ni2–O9	2.061(4)	Ni4–O6	2.067(3)
Ni2–O1	2.098(3)	Ni4–O1	2.205(3)

Table 4. Ni–O–Ni Angles (deg) for 2·H_2O and 3·$4H_2O$

2·H_2O			
Ni1–O2–Ni2	104.5(2)	Ni2–O4–Ni4	91.4(2)
Ni1–O2–Ni3	95.3(2)	Ni2–O3–Ni4	94.6(2)
Ni1–O1–Ni4	98.3(2)	Ni2–O2–Ni3	98.5(2)
Ni1–O1–Ni3	92.0(2)	Ni2–O3–Ni3	99.5(2)
Ni1–O4–Ni2	97.5(2)	Ni3–O1–Ni4	97.0(2)
Ni1–O4–Ni4	98.9(2)	Ni3–O3–Ni4	104.7(2)
3·$4H_2O$			
Ni1–O5–Ni2	94.1(1)	Ni2–O4–Ni3	99.2(1)
Ni1–O5–Ni3	103.6(1)	Ni2–O4–Ni4	103.1(1)
Ni1–O6–Ni3	94.0(1)	Ni2–O1–Ni4	94.5(1)
Ni1–O6–Ni4	100.6(1)	Ni2–O5–Ni3	99.9(1)
Ni1–O1–Ni2	89.5(1)	Ni3–O4–Ni4	94.5(1)
Ni1–O1–Ni4	101.0(1)	Ni3–O6–Ni4	90.3(1)

$\{Ni_4O_4\}$ units, consisting of two interpenetrating Ni_4 and O_4 tetrahedra, with different degrees of distortion of the cubane motif (Supporting Information Figure S8). Two of the six faces of the $\{Ni_4O_4\}$ cube are distinctly different, being spanned by capping carboxylates that result in somewhat different bond lengths and angles for the involved atoms (Table 3 and Table S1 in Supporting Information) compared to those at the four remaining faces of the $\{Ni_4O_4\}$ cube which are spanned by $\mu_{1,3}$-carboxylato bridges. The six Ni···Ni distances fall within 2.937–3.303 Å range. The faces spanned by $\mu_{1,3}$-O_2CCF_3 units in **2**·H_2O register Ni···Ni separations of 2.962 and 2.979 Å, while the corresponding faces spanned by $\mu_{1,3}$-O_2CCH_2Ph in **3**·$4H_2O$ show separations of 2.937 and 2.944 Å. In these two faces the Ni^{II} ions are triply bridged. The Ni···Ni distances bridged by two HO^-

dx.doi.org/10.1021/ic401337q | Inorg. Chem. 2013, 52, 13894–13903

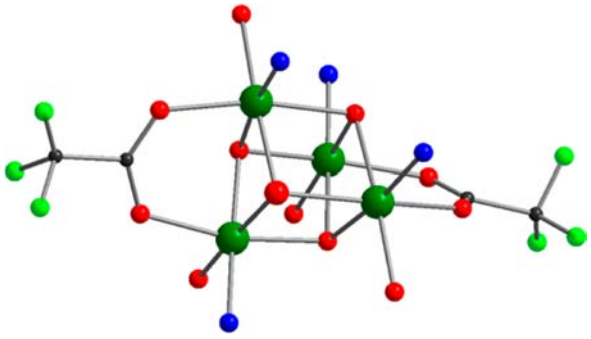

Figure 5. Atom connectivity in the core of complex **2**·H_2O showing octahedral coordination for all Ni^{II} atoms. Color code: Ni, dark green; O, red; N, blue; C, black.

groups are intermediate at 3.090 and 3.098 Å for **2**·H_2O and **3**·$4H_2O$, respectively. The binding of two $CF_3CO_2^-$ and two $PhCH_2CO_2^-$ ions is different as reflected in the Ni−O distances in 2.055−2.148 and 2.033−2.077 Å ranges (Supporting Information Figure S9). In both cubane complexes the primary chelating Schiff base ligands are present in their singly deprotonated form H_2pbmp^-, and the Ni−O (hydroxide) and Ni−N (imine) distances are similar, within 1.987−2.050 Å. The μ_3-PhO^- group links two Ni^{II} atoms in one face of the cube and extends the third arm to another Ni^{II} atom of the other plane. The former Ni−O bonds (~2.06 Å) are shorter compared to the latter (~2.20 Å). The O1(phenoxido) and O4(phenoxide) donor atoms of this group lie 1.092 and 1.085 Å out of the plane of the three connected Ni^{II} atoms: the solid angles around these atoms are 299.3° and 298.9° and two of the Ni−O−Ni angles are significantly larger (104.9° and 98.8°; 104.6° and 99.5°) than the third one (95.5°; 94.5°). The Ni−O(H) bonds from alcohol terminal ends are comparatively shorter in 2.02−2.08 Å range.

An interesting feature of complexes **2**·H_2O and **3**·$4H_2O$ is the packing of the cubane clusters by hydrogen bonds between the bridging HO^- ions and lattice H_2O molecules, which act as hydrogen bond donors, and the O atoms of carboxylate anions present nearby that act as hydrogen bond acceptors. The cationic complex **2**·H_2O crystallizes with two trifluoroacetate anions and two solvent water molecules which are hydrogen bonded to one bridging hydroxide group and two pendent ligand alcohol arms (Supporting Information Figure S10). The hydroxido anions (O2 and O3) of **2**·H_2O function as hydrogen bond donors to carboxylate O16 and O14 resulting in O···O separations of 2.820 and 2.738 Å, respectively. The lattice water oxygen atom (O2W) shows hydrogen bonding with O6 of ligand alcohol arm with O···O separation of 2.672 Å. The pendent and protonated ligand alcohol arms O5 and O8 are hydrogen bonded to O15 and O13 of lattice trifluoroacetate anions showing O···O separation of 2.618 and 2.594 Å, respectively (Supporting Information Figures S10 and S11). The dication of **3**·$4H_2O$ crystallizes with two phenyl acetate anions and four solvent water molecules and shows hydrogen bonding with bridging hydroxide groups and OH bearing ligand alcohol arms (Supporting Information Figure S12). Hydrogen bonding interactions of $PhCH_2CO_2^-$ ions and water molecules with the cubane dication in **3**·$4H_2O$ pertain extra stability to the crystal structure. One of the lattice water oxygen atoms (O1W) is hydrogen bonded to lattice carboxylate oxygen atom (O13) at 2.791 Å O···O separation. The other lattice water oxygen atom (O2W) shows hydrogen bonding with lattice carboxylate oxygen atom (O14) at 2.734 Å and with hydroxido bridge O3 atom at 2.846 Å. The O atoms of the phenyl acetate anions (O13 and O14) are close to terminal alcohol O2 atom (O···O, 2.573 Å) (Supporting Information Figure S13).

Magnetic Properties. Magnetic measurements were performed on polycrystalline samples of **1**−**3**. All three complexes exhibit room-temperature χT values that are slightly higher than the expected spin-only value of 1.00 emu K mol^{-1} per one Ni(II) ion (S = 1). Such behavior is typical for Ni(II) complexes and explained by the orbital contribution to the total magnetic moment.[34]

Complex **1** exhibits the χT value of 6.93 emu K mol^{-1} at 300 K (Figure 6). The χT slightly increases as the temperature is lowered, reaching the maximum of 7.65 emu K mol^{-1} at 26 K, after which it sharply decreases to 4.32 emu K mol^{-1} at 1.8 K, the lowest temperature available in our experiments. The magnetization (M) measured at 1.8 K exhibits a gradual increase with the increasing field (H) but does not reach saturation even at 7 T (Figure 6, inset). The character of $\chi T(T)$ and $M(H)$ dependences suggests the presence of competing magnetic interactions in **1**. The magnetic behavior of **1** was modeled with the isotropic Heisenberg−Dirac−Van Vleck (HDV) Hamiltonian, including the zero-field and Zeeman splitting effects:

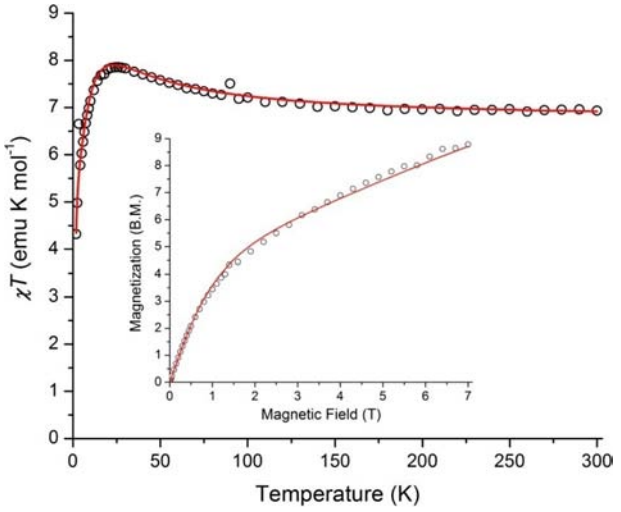

Figure 6. Temperature dependence of χT for **1**. Inset: Field-dependent magnetization at 1.8 K. Solid red lines correspond to the theoretical simulation.

$$\hat{H} = -\sum_{i<j} 2J_{ij}\hat{S}_i\hat{S}_j + \sum_i D_i[\hat{S}_{z,i}^2 - S_i(S_i + 1)/3] + \sum_i g_i\mu_B\hat{S}_i\vec{H} \quad (4)$$

where i and j are used to specify the five Ni(II) centers, D_i is the single-ion zero-field splitting parameter, H is the applied magnetic field, and μ_B is Bohr magneton. Given the symmetry of complex **1**, the similarity of Ni1···Ni2 and Ni1···Ni3 distances (3.617 and 3.608 Å, respectively), and the long Ni2···Ni3* and Ni3···Ni2* separations of 6.595 Å (Figure 2), eq 4 can be simplified by using only two magnetic exchange constants and assuming the same value of g and D for all Ni(II) ions to avoid overparametrization:

dx.doi.org/10.1021/ic401337q | Inorg. Chem. 2013, 52, 13894−13903

$$\hat{H} = -2J_1(\hat{S}_{Ni2}\hat{S}_{Ni3} + \hat{S}_{Ni2*}\hat{S}_{Ni3*}) - 2J_2(\hat{S}_{Ni1}\hat{S}_{Ni2} + \hat{S}_{Ni1}\hat{S}_{Ni3} + \hat{S}_{Ni1}\hat{S}_{Ni2*} + \hat{S}_{Ni1}\hat{S}_{Ni3*}) + 5D[\hat{S}_z^2 - S(S+1)/3] + 5g\mu_B\hat{S}\vec{H} \quad (5)$$

The magnetic data were satisfactorily simulated with Magpack[35] (red lines in Figure 6), resulting in $J_1 = 7.0(5)$ cm^{-1}, $J_2 = -0.7(1)$ cm^{-1}, $D = 8.3(2)$ cm^{-1}, $g = 2.32(1)$. The latter two values are typical of Ni(II) complexes.[34] The simulation indicates a moderate ferromagnetic exchange along the oxo-bridged Ni2−Ni3 and Ni2*−Ni3* sides of the Ni_5 rectangle and a weaker antiferromagnetic coupling between the corner ions and the central Ni1 ion. The maximum magnetization value achieved at 1.8 K and 7 T is 8.7 μ_B, much higher than 6 μ_B expected for the ground state of $S_T = 3$. Moreover, the magnetization gradually increases at higher fields, suggesting that the applied magnetic field suppresses the antiferromagnetic exchange between the central Ni1 ion and the four corner ions. An examination of AC magnetic susceptibility did not reveal any out-of-phase signal, indicating the absence of single-molecule magnetism in this complex.

The room-temperature χT value for **2** is 5.59 emu K mol^{-1} at 300 K (Figure 7). Similar to complex **1**, the χT of **2** slowly

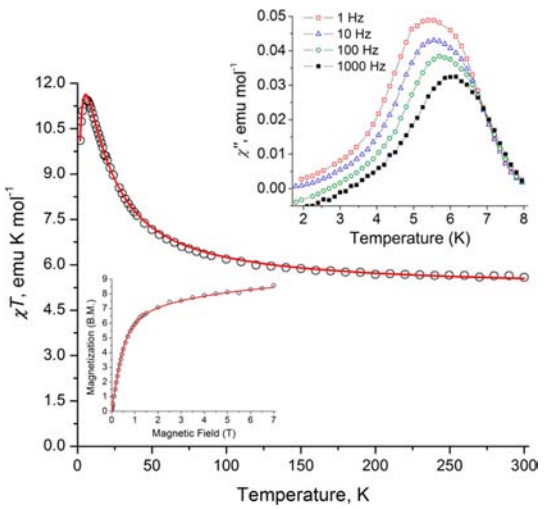

Figure 7. Temperature dependence of χT for **2**. Insets: Bottom, field-dependent magnetization at 1.8 K; top, imaginary part of AC magnetic susceptibility. Solid red lines correspond to the theoretical simulation.

increases as the temperature is decreased, but the increase at lower temperatures is much more abrupt and the maximum value of 11.4 emu K mol^{-1} is reached at 6.6 K. The field-dependent magnetization measured at 1.8 K exhibits fast growth with increasing field and approaches the saturation value of ~8.6 μ_B at 7 T (Figure 7, bottom inset). Such behavior suggests dominant ferromagnetic interactions in the cubane cluster of **2**, with the stabilization of the $S_T = 4$ ground state at low temperature, and agrees with the behavior reported previously for similar Ni(II) cubane clusters.[36] Taking into account that Ni1···Ni3 and Ni2···Ni4 distances (2.979 and 2.962 Å, respectively) are notably shorter than the other four Ni···Ni separations (>3.09 Å) in the Ni_4O_4 core of the cubane unit (Supporting Information Figure S8), the magnetic behavior of **2** was modeled with two values of J. Initially, the spin-only Hamiltonian

$$\hat{H} = -2J_1(\hat{S}_1\hat{S}_3 + \hat{S}_2\hat{S}_4) - 2J_2(\hat{S}_1\hat{S}_2 + \hat{S}_1\hat{S}_4 + \hat{S}_2\hat{S}_3 + \hat{S}_3\hat{S}_4) + 4g\mu_B\hat{S}\vec{H} \quad (6)$$

was solved analytically using the Kambe method.[36] The corresponding energy eigenvalues,

$$E = -J_1[S_A(S_A+1) + S_B(S_B+1)] - J_2[S_T(S_T+1) - S_A(S_A+1) - S_B(S_B+1)] \quad (7)$$

where $\hat{S}_A = \hat{S}_1 + \hat{S}_3$, $\hat{S}_B = \hat{S}_2 + \hat{S}_4$, and $\hat{S}_T = \hat{S}_A + \hat{S}_B$, were entered into the Van Vleck equation

$$\chi T = \frac{Ng^2}{3k}\sum_i \frac{S_T(S_T+1)(2S_T+1)e^{-E_i/kT}}{(2S_T+1)e^{-E_i/kT}} \quad (8)$$

to fit the experimental $\chi T(T)$ curve above 8 K. This procedure provided the best-fit values of magnetic parameters, $J_1 = 9.3$ cm^{-1}, $J_2 = 1.1$ cm^{-1}, and $g = 2.27$. Subsequently, these were used as the initial values for the Magpack simulation that took into account the zero-field splitting effects, according to the Hamiltonian

$$\hat{H} = -2J_1(\hat{S}_1\hat{S}_3 + \hat{S}_2\hat{S}_4) - 2J_2(\hat{S}_1\hat{S}_2 + \hat{S}_1\hat{S}_4 + \hat{S}_2\hat{S}_3 + \hat{S}_3\hat{S}_4) + 4D[\hat{S}_z^2 - S(S+1)/3] + 4g\mu_B\hat{S}\vec{H} \quad (9)$$

The best simulation of the experimental data was obtained with $J_1 = 8.4(2)$ cm^{-1}, $J_2 = 1.05(3)$ cm^{-1}, $D = 7.8(2)$ cm^{-1}, $g = 2.28(1)$ (red lines in Figure 7).

An examination of AC magnetic susceptibility of **2** reveals an appearance of an out-of-phase signal with a frequency-dependent maximum, indicating that complex **2** exhibits the slow relaxation of magnetization. A number of cubane clusters with the Ni_4O_4 core have been shown to undergo the frequency-dependent relaxation of magnetization indicative of SMM behavior,[36a,b,d] but for all these clusters the blocking temperature is usually quite low (<3 K) because of fast magnetization tunneling in zero field.[37] In the present case, however, the blocking temperature appeared to be unusually high, ~5.5 K. The relaxation rate was fit to the Arrhenius law, $\ln(\tau_0/\tau) = -U_{eff}/kT$, where $\tau = 2\pi\nu$, to allow the estimation of the pre-exponential rate constant, $1/\tau_0 = 1.2(1)\cdot10^{-31}$ s^{-1}, and the effective barrier to the relaxation of magnetization, $U_{eff} = 296(2)$ cm^{-1}. These values are somewhat extreme for conventional SMMs. The Mydosh parameter, an empirical quantity used to differentiate between superparamagnets and spin glasses, was calculated as $\varphi = (T_{max}^{\nu_1} - T_{max}^{\nu_2})/(T_{max}^{\nu_1}(\log\nu_1 - \log\nu_2))$, where $T_{max}^{\nu_i}$ is the temperature of the maximum in the χ'' versus T curve at the corresponding frequency.[38] This calculation led to $\varphi = 0.034$, which falls in the range typical for spin glasses (0.004−0.08).

Taking into account the substantial separation between the clusters in the solid state, it is intriguing to see the signature of spin glassiness at the temperature as high as 5.5 K, because such behavior implies non-negligible intercluster magnetic coupling. Nevertheless, the $[Ni_4O_4]$ cubanes were shown to exhibit exchange bias due to intermolecular interactions.[39] The possibility of the more pronounced coupling could be envisioned in the structure of **2**, with the relatively nonbulky trifluoroacetate ligands, if the structure underwent some collapse/disorder upon the loss of interstitial solvent. Indeed, a visual examination of the microcrystalline samples revealed the presence of powder-like deposit on the surface of the crystallites. Consequently, the crystals were ground into a fine powder, which caused the increase in the maximum value of χ'' from 0.049 to 0.076 emu

dx.doi.org/10.1021/ic401337q | Inorg. Chem. 2013, 52, 13894−13903

mol^{-1}. This increase suggests that the spin-glass behavior is due to the coupling between the $S = 4$ clusters in the disordered structure formed upon the loss of interstitial solvent.

The magnetic behavior of **3** (Figure 8 and Supporting Information Figure S14) was found to be similar to that of **2**, as

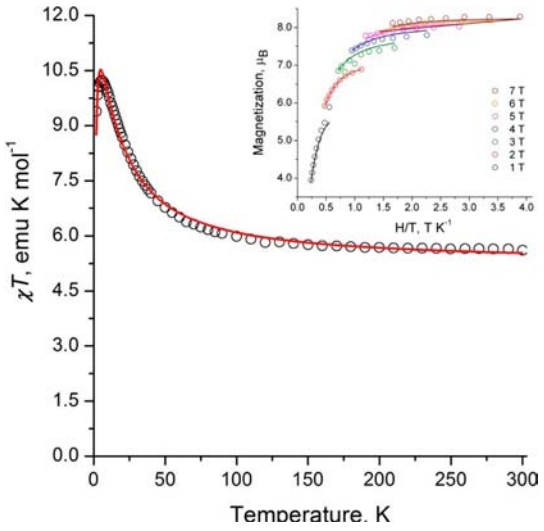

Figure 8. Temperature dependence of χT for **3**. Inset: Reduced magnetization plot, with solid lines representing the best theoretical fit ($g = 2.09$, $D = -0.39$ cm^{-1}).

expected from the structural similarity of the $[Ni_4O_4]$ cubane core in these complexes. Simulating $\chi T(T)$ and $M(H)$ curves of **3** with Magpack according to eq 9, in the manner analogous to that described above for **2**, resulted in comparable values of magnetic parameters, $J_1 = 7.2(2)$ cm^{-1}, $J_2 = 0.60(5)$ cm^{-1}, $D = 8.5(2)$ cm^{-1}, $g = 2.29(1)$. An examination of AC magnetic susceptibility of **3** did not reveal any slow relaxation process in the range of 1.8−9.0 K, indicating that, in contrast to **2**, this complex exhibits neither spin-glass nor SMM behavior. On one hand, the bulkier phenylacetate ligands provide a more robust crystal packing and larger separation between the $[Ni_4O_4]$ clusters in **3**, thus preventing any significant intercluster magnetic exchange. On the other hand, the lack of the SMM behavior can be explained by the relatively low symmetry of the cubane core in **3**, which results in fast tunneling of magnetization. Consequently, the AC susceptibility of **3** was examined under DC bias field of 0.2 T, which led to the appearance of an out-of-phase frequency-dependent peak around 2.5 K (Supporting Information Figure S14, inset), indicating that the tunneling is suppressed due to field-induced energy mismatch for the $+M_S$ and $-M_S$ magnetic states.

The ground-state properties of **3** were examined by variable-temperature magnetization measurements under different applied magnetic fields (Figure 8, inset). The fit of the reduced magnetization data was performed with Anisofit,[40] resulting in the best-fit values of $g = 2.09$ and $D = -0.39$ cm^{-1} for the $S = 4$ ground state of the Ni_4 cubane. These values are similar to those reported for other Ni_4O_4 clusters,[36] and the negative value of D agrees with the observation of the out-of-phase signal under applied magnetic field.

CONCLUSION

The use of phenol function deprotonated H_2bpmp^- ligand with three different Ni(II) carboxylates has provided access to three new self-assembled coordination cages following in situ generation of HO^- ions from water present in the reaction medium. Complex **1** reveals an unusual structure having five nickel(II) ions in an hourglass arrangement hitherto unknown in coordination cluster chemistry of H_2bpmp^- with nickel(II). The complex has a ground-state spin of $S = 3$. The synthesis and stability in its pentanuclear form is dependent on the particular nature of the R group on the carboxylate group required for bridging. Thus moving from propanoate group to trifluoroacetate and phenylaceate groups provided different course of cluster assembly based on binuclear motifs. This carboxylate bridging induced cluster assembly allowed synthesizing new family of hydroxido-bridged tetranuclear Ni^{II} cube structures **2** and **3**. Change of face-capping carboxylato groups is accompanied by slight structural rearrangement of the $[Ni_4O_4]$ core, which in turn results in changes in magnetic behavior. Simultaneous chelation of binucleating H_2bpmp^- and bridging of water-derived HO^- groups in μ_3 mode, in presence of two carboxylate anions lead to the generation of two $[Ni_4O_4]$ cubane complexes exhibiting three different types of Ni_2O_2 faces having Ni···Ni separations in the ranges of 2.93−2.97, 3.09−3.21, and 3.20−3.30 Å, respectively. The differences in the bulkiness of carboxylate ligands in **2** and **3** lead to the weakening of intercluster magnetic exchange interactions in the latter. As a result, complex **2** exhibits spin-glass behavior upon the loss of interstitial solvent, while complex **3** shows slow relaxation of magnetization, but only when a DC magnetic field is applied to suppress the fast tunneling between the states of opposite magnetization direction.

ASSOCIATED CONTENT

Supporting Information

X-ray crystallographic data in CIF format, Scheme S1, Figures S1−S13, Table S1, and synthesis and characterization of ligand H_3bpmp. This material is available free of charge via the Internet at http://pubs.acs.org.

AUTHOR INFORMATION

Corresponding Author

*Fax: (+91) 3222-82252. Tel: (+91) 3222-283324. E-mail: dray@chem.iitkgp.ernet.in.

Notes

The authors declare no competing financial interest.

ACKNOWLEDGMENTS

A.K.G. is thankful to the Council of Scientific and Industrial Research, New Delhi, India for financial support. The authors also give thanks to DST, New Delhi, for providing the Single Crystal X-ray Diffractometer facility in the Department of Chemistry, IIT Kharagpur under its FIST program. V.B. acknowledges the Italian Ministry of University and Scientific Research (MIUR, Rome). M.S. is grateful to the National Science Foundation for the partial support of this work (award CHE-0911109).

REFERENCES

(1) Kostakis, G. E.; Ako, A. M.; Powell, A. K. *Chem. Soc. Rev.* **2010**, *39*, 2238.

(2) (a) Christou, G.; Gatteschi, D.; Hendrickson, D. N.; Sessoli, R. *MRS Bull.* **2000**, 66. (b) Krzystek, J.; Telser, J.; Pardi, L. A.; Goldberg, D. P.; Hoffman, B. M.; Brunel, L.-C. *Inorg. Chem.* **1999**, *38*, 6121.

(3) (a) Chen, S.-Y.; Beedle, C. C.; Gan, P.-R.; Lee, G.-H.; Hill, S.; Yang, E.-C. *Inorg. Chem.* **2012**, *51*, 4448. (b) Caneschi, A.; Gatteschi, D.;

Sessoli, R.; Barra, A. L.; Brunel, L. C.; Guillot, M. *J. Am. Chem. Soc.* **1991**, *113*, 5873. (c) Aubin, S. M. J.; Dilley, N. R.; Pardi, L.; Krzystek, J.; Wemple, M. W.; Brunel, L.-C.; Maple, M. B.; Christou, G.; Hendrickson, D. N. *J. Am. Chem. Soc.* **1998**, *120*, 4991. (d) Christou, G.; Gatteschi, D.; Hendrickson, D. N.; Sessoli, R. *MRS Bull.* **2000**, *25*, 66. (e) Gatteschi, D.; Sessoli, R. *Angew. Chem., Int. Ed.* **2003**, *42*, 268. (f) Oshio, H.; Nakano, M. *Chem.—Eur. J.* **2005**, *11*, 5178. (g) Bircher, R.; Chaboussant, G.; Dobe, C.; Gudel, H. U.; Ochsenbein, S. T.; Sieber, A.; Waldmann, O. *Adv. Funct. Mater.* **2006**, *16*, 209. (h) Aromí, G.; Brechin, E. K. *Struct. Bonding (Berlin)* **2006**, *122*, 1. (i) Powell, A. K. *Nat. Chem.* **2010**, *2*, 351.

(4) (a) Stamatatos, T. C.; Adam, R.; Raptopoulou, C. P.; Psycharis, V.; Ballesteros, R.; Abarca, B.; Perlepes, S. P.; Boudalis, A. K. *Inorg. Chem. Commun.* **2012**, *15*, 73. (b) Tasiopoulos, A. J.; Vinslava, A.; Wernsdorfer, W.; Abboud, K. A.; Christou, G. *Angew. Chem., Int. Ed.* **2004**, *43*, 2117. (c) Liu, T.; Zhang, Y.-J.; Wang, Z.-M.; Gao, S. *J. Am. Chem. Soc.* **2008**, *130*, 130. (d) Lee, C.-F.; Leigh, D. A.; Pritchard, R. G.; Schultz, D.; Teat, S. J.; Timco, G. A.; Winpenny, R. E. P. *Nature* **2009**, *458*, 314.

(5) Robson, G.; Butler, T. *Int. J. Urban Reg. Res.* **2001**, *.25.1*, 70.

(6) Rey, N. A.; Neves, A.; Bortoluzzi, A. J.; Pich, C. T.; Terenzi, H. *Inorg. Chem.* **2007**, *46*, 348.

(7) Sarkar, M.; Clérac, R.; Mathonière, C.; Hearns, N. G. R.; Bertolasi, V.; Ray, D. *Inorg. Chem.* **2010**, *49*, 6575.

(8) Sarkar, M.; Clérac, R.; Mathonière, C.; Hearns, N. G. R.; Bertolasi, V.; Ray, D. *Inorg. Chem.* **2011**, *50*, 3922.

(9) (a) Das, A.; Klinke, F. J.; Demeshko, S.; Meyer, S.; Dechert, S.; Meyer, F. *Inorg. Chem.* **2012**, *51*, 8141. (b) Mandal, D.; Hong, C. S.; Kim, H. C.; Fun, H.-K.; Ray, D. *Polyhedron* **2008**, *27*, 2372. (c) Bechlars, B.; Issac, I.; Feuerhake, R.; Clérac, R.; Fuhr, O.; Fenske, D. *Eur. J. Inorg. Chem.* **2008**, 1632.

(10) Liu, S.; Wang, S.; Cao, F.; Fu, H.; Li, D.; Dou, J. *RSC Adv.* **2012**, *2*, 1310.

(11) (a) King, P.; Clérac, R.; Wernsdorfer, W.; Anson, C. E.; Powell, A. K. *Dalton Trans.* **2004**, 2670. (b) Mondal, K. C.; Sengupta, O.; Mukherjee, P. S. *Inorg. Chem. Commun.* **2009**, *12*, 682.

(12) (a) Zhao, F.-H.; Che, Y.-X.; Zheng, J.-M. *Cryst. Growth Des.* **2012**, *12*, 4712. (b) Papatriantafyllopoulou, C.; Stamatatos, T. C.; Wernsdorfer, W.; Teat, S. J.; Tasiopoulos, A. J.; Escuer, A.; Perlepes, S. P. *Inorg. Chem.* **2010**, *49*, 10486. (c) Wei, Y.; Hou, H.; Fan, Y.; Zhu, Y. *Eur. J. Inorg. Chem.* **2004**, 3946. (d) Aromí, G.; Bell, A. R.; Helliwell, M.; Raftery, J.; Teat, S. J.; Timco, G. A.; Roubeau, O.; Winpenny, R. E. P. *Chem.—Eur. J.* **2003**, *9*, 3024. (e) Malkov, A. E.; Fomina, I. G.; Sidorov, A. A.; Aleksandrov, G. G.; Egorov, I. M.; Latosh, N. I.; Chupakhin, O. N.; Rusinov, G. L.; Rakitin, Yu. Y.; Novotortsev, V. M.; Ikorskii, V. N.; Eremenko, I. L.; Moiseev, I. I. *J. Mol. Struct.* **2003**, *656*, 207. (f) Finney, A. J.; Hitchman, M. A.; Raston, C. L.; Rowbottom, G. L.; White, A. H. *Aust. J. Chem.* **1981**, *34*, 3139.

(13) Tandon, S. S.; Bunge, S. D.; Rakosi, R.; Xu, Z.; Thompson, L. K. *Dalton Trans.* **2009**, 6536.

(14) Weinstock, I. A. *Chem. Rev.* **1998**, *98*, 113.

(15) (a) Esteban, J.; Ruiz, E.; Font-Bardia, M.; Calvet, T.; Escuer, A. *Chem.—Eur. J.* **2012**, *18*, 3637. (b) Scheurer, A.; Gieb, K.; Alam, M. S.; Heinemann, F. W.; Saalfrank, R. W.; Kroener, W.; Petukhov, K.; Stockerb, M.; Müller, P. *Dalton Trans.* **2012**, *41*, 3553. (c) Petit, S.; Neugebauer, P.; Pilet, G.; Chastanet, G.; Barra, A.-L.; Antunes, A. B.; Wernsdorfer, W.; Luneau, D. *Inorg. Chem.* **2012**, *51*, 6645. (d) Stamatatos, T. C.; Escuer, A.; Abboud, K. L.; Raptopoulou, C. P.; Perlepes, S. P.; Christou, G. *Inorg. Chem.* **2008**, *47*, 11825. (e) Escuer, A.; Esteban, J.; Roubeau, O. *Inorg. Chem.* **2010**, *50*, 8893.

(16) (a) Mukherjee, S.; Weyhermüller, T.; Bothe, E.; Wieghardt, K.; Chaudhuri, P. *Eur. J. Inorg. Chem.* **2003**, 863. (b) Papatriantafyllopoulou, C.; Stamatatos, T. C.; Wernsdorfer, W.; Teat, S. J.; Tasiopoulos, A. J.; Escuer, A.; Perlepes, S. P. *Inorg. Chem.* **2010**, *49*, 10486. (c) Escuer, A.; Vlahopouloua, G.; Mautnerb, F. A. *Dalton Trans* **2011**, *40*, 10109. (d) Pons-Balague, A.; Ioanidis, N.; Wernsdorfer, W.; Yamaguchi, A.; Sanudo, E. C. *Dalton Trans.* **2011**, *40*, 11765.

(17) Sarkar, A.; Ghosh, A. K.; Bertolasi, V.; Ray, D. *Dalton Trans.* **2012**, *41*, 1889.

(18) Mandal, D.; Bertolasi, V.; Ribas-Ariño, J.; Aromí, G.; Ray, D. *Inorg. Chem.* **2008**, *47*, 3465.

(19) Gagne, R. R.; Spiro, C. L.; Smith, T. J.; Hamann, C. A.; Thies, W. R.; Shiemke, A. K. *J. Am. Chem. Soc.* **1981**, *103*, 4073.

(20) Bain, G. A.; Berry, J. F. *J. Chem. Educ.* **2008**, *85*, 532.

(21) Otwinowski, Z.; Minor, W. In *Methods in Enzymology*; Carter, C. W., Sweet, R. M., Eds.; Academic Press: London, 1997; Vol. *276*, Part A, p 307.

(22) Blessing, R. H. *Acta Crystallogr., Sect. A* **1995**, *51*, 33.

(23) Altomare, A.; Burla, M. C.; Camalli, M.; Cascarano, G. L.; Giacovazzo, C.; Guagliardi, A.; Moliterni, A. G.; Polidori, G.; Spagna, R. *J. Appl. Crystallogr.* **1999**, *32*, 115.

(24) Sheldrick, G. M. *SHELX-97, Program for Crystal Structure Refinement*; University of Göttingen: Göttingen, Germany, 1997.

(25) Nardelli, M. *J. Appl. Crystallogr.* **1995**, *28*, 659.

(26) Farrugia, L. J. *J. Appl. Crystallogr.* **1999**, *32*, 837.

(27) (a) Chowdhury, P. K. S.; Mukhopadhyay, U.; Ray, D. *Indian J. Chem.* **1999**, *38A*, 1159. (b) Mandal, D.; Bertolasi, V.; Aromi, G.; Ray, D. *Dalton Trans.* **2007**, 1989.

(28) Deacon, G. B.; Phillips, R. J. *Coord. Chem. Rev.* **1980**, *33*, 227.

(29) Clemente-Juan, J. M.; Chansou, B.; Donnadieu, B.; Tuchagues, J.-P. *Inorg. Chem.* **2000**, *39*, 5515.

(30) Tomkowicz, Z.; Ostrovsky, S.; H. Muller-Bunz, H.; Eltmimi, A. J. H.; M. Rams, D. A.; Brown, D. A.; Haase, W. *Inorg. Chem.* **2008**, *47*, 6956.

(31) Salawu, O. W.; Aliyu, A. O. C. *Adv. Pure Appl. Chem.* **2012**, *1*, 2167.

(32) Paital, A. R.; Mikuriya, M.; Ray, D. *Eur. J. Inorg. Chem.* **2007**, 5360.

(33) (a) Mukherjee, P.; Drew, M. G. B.; Gómez-García, C. J; Ghosh, A. *Inorg. Chem.* **2009**, *48*, 4817−4827. (b) Biswas, R.; Ida, Y.; Baker, M. L.; Biswas, S.; Kar, P.; Nojiri, H.; Ishida, T.; Ghosh, A. *Chem.—Eur. J.* **2013**, *19*, 3943−3953.

(34) Carlin, R. L. *Magnetochemistry*; Springer-Verlag: Berlin, Germany, 1986.

(35) Borrás-Almenar, J.; Clemente-Juan, J. M.; Coronado, E.; Tsukerblat, B. S. *J. Comput. Chem.* **2001**, *22*, 985.

(36) (a) Yang, E.-C.; Wernsdorfer, W.; Zakharov, L. N.; Karaki, Y.; Yamaguchi, A.; Isidro, R. M.; Lu, G.-D.; Wilson, S. A.; Rheingold, A. L.; Ishimoto, H.; Hendrickson, D. N. *Inorg. Chem.* **2006**, *45*, 529. (b) Yang, E.-C.; Wernsdorfer, W.; Hill, S.; Edwards, R. S.; Nakano, M.; Maccagnano, S.; Zakharov, L. N.; Rheingold, A. L.; Christou, G.; Hendrickson, D. N. *Polyhedron* **2003**, *22*, 1727. (c) Zhang, S.-H.; Li, N.; Ge, C.-M.; Feng, C.; Ma, L.-F. *Dalton Trans.* **2011**, *40*, 3000. (d) Moragues-Cánovas, M.; Helliwell, M.; Ricard, L.; Rivière, É.; Wernsdorfer, W.; Brechin, E.; Mallah, T. *Eur. J. Inorg. Chem.* **2004**, 2219.

(37) Hendrickson, D. N.; Yang, E.-C.; Isidro, R. M.; Kirman, C.; Lawrence, J.; Edwards, R. S.; Hill, S.; Yamaguchi, A.; Ishimoto, H.; Wernsdorfer, W.; Ramsey, C.; Dalal, N. S.; Olmstead, M. M. *Polyhedron* **2005**, *24*, 2280.

(38) Mydosh, J. A. *Spin Glasses: An Experimental Introduction*; Taylor & Francis: Washington, DC, 1993.

(39) Ferguson, A.; Lawrence, J.; Parkin, A.; Sanchez-Benitez, J.; Kamenev, K. V.; Brechin, E. K.; Wernsdorfer, W.; Hill, S.; Murrie, M. *Dalton Trans.* **2008**, 6409.

(40) Shores, M. P.; Sokol, J. J.; Long, J. R. *J. Am. Chem. Soc.* **2002**, *124*, 2279−2292.